THE JOURNAL OF PHYSICAL CHEMISTRY B

pubs.acs.org/JPCB Article

A Quantitatively Accurate Theory to Predict Adsorbed Configurations of Asymmetric Surfactant Molecules on Polar Surfaces

Xueying Ko and Sumit Sharma*

Cite This: https://dx.doi.org/10.1021/acs.jpcb.0c02681 Read Online

ACCESS | Metrics & More | Article Recommendations | Supporting Information

ABSTRACT: We introduce a theoretical model that predicts adsorbed configurations of asymmetric surfactant molecules on polar surfaces. This model extends the ideas developed in our previous work for predicting adsorbed configurations of linear surfactant molecules on polar surfaces. The surfactant molecules have a large polar headgroup and a linear alkyl tail. These asymmetric molecules form cylindrical/spherical morphologies in the adsorbed state. Our model predicts that the molecules adsorb either with their molecular axis parallel to the surface (lying-down configuration) or perpendicular to the surface (standing-up configuration). The standing-up and lying-down configurations result in significantly different adsorbed morphologies. In the standing-up configuration, the adsorbed morphology is like that of full cylinders, while, in the lying-down configuration, the adsorbed morphology resembles partial spheres. The standing-up configuration is obtained when the strength of interaction of the polar headgroup with the surface dominates over the interactions of the alkyl tail with the surface. When interactions of the alkyl tail are dominant, the molecules attain the lying-down configuration. Predictions from the theoretical model quantitatively match the results obtained from Langevin dynamics simulations. The theoretical model also explains the different kinetic pathways that have been reported in the experimental studies on the organization of adsorbed surfactants on polar surfaces.

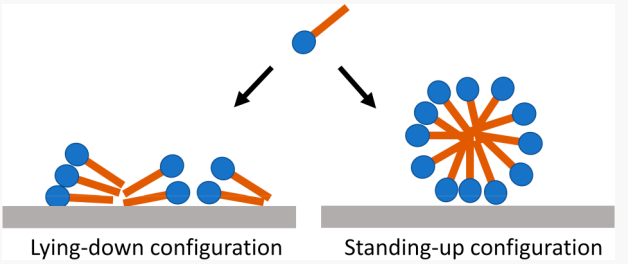

1. INTRODUCTION

Adsorption of surfactants on metal surfaces is useful in many applications, including inhibition of corrosion in oil and gas pipelines,[1] modulating electrochemical reactions,[2] tuning the selectivity of chemical reactions,[3] and synthesis of anisotropic metal nanoparticles of desired shapes and sizes.[4] The adsorption mechanism can be thought of as being comprised of two processes: the diffusion of surfactants toward the surface and the organization of adsorbed molecules. Surfactants aggregate as micelles above the critical micelle concentration (CMC), and experiments report a change in the adsorption kinetics as the concentration increases above the CMC.[5] These results are rationalized via atomistic simulations that have shown that surfactant micelles experience a free energy barrier to adsorption on metal surfaces, which is absent in the case of unaggregated molecules.[6−8] Upon adsorption, surfactant molecules are understood to organize themselves in various structures or morphologies, including planar films,[9,10] (hemi-) cylinders, and (hemi-) spheres.[11−13] These morphologies are expected to affect the interfacial properties differently.[14] Therefore, understanding the factors that result in the formation of different adsorption morphologies will be useful for the purpose of rational design of surfactants for specific applications. A pioneering work focused on predicting the morphologies of adsorbed surfactants via macroscopic thermodynamic theory has been done by Nagarajan and co-workers.[15,16] However, an encompassing theoretical framework that is able to predict adsorbed morphologies of surfactants on polar surfaces directly from molecular properties and surfactant−surface interactions has not been established.

Experiments have shown that the organization of adsorbed surfactants on polar surfaces can occur via different kinetic pathways. The first kind of pathway, as reported for the adsorption of alkanethiols on gold,[10,17] is comprised of two steps. In the first step, the molecules adsorb by lying flat with their axis parallel to the surface to form a stripe-like configuration. This is followed by an orientational transition wherein the molecules stand up on the surface, allowing for more molecules to adsorb.[10,17] The second kind of pathway, for instance, reported for the adsorption of octadecylphosphonic acid[18,19] and octadecyltrimethylammonium bromide (C_{18}TAB)[20] on mica, involves nucleation of densely packed molecular islands on the surface. As the adsorption proceeds,

Received: March 26, 2020
Revised: May 7, 2020
Published: June 8, 2020

these islands grow and coalesce to form a contiguous layer on the surface.

In our previous work, we developed a theoretical model for predicting adsorbed configurations of linear surfactant molecules on polar surfaces.[21] We demonstrated, via molecular simulations, that our theoretical model is quantitatively accurate in its predictions. However, an outstanding question remained if our model can be extended to asymmetrical surfactant molecules that form more complex, nonplanar adsorption morphologies. In this work, we extend our theoretical model to asymmetric surfactant molecules that have a linear alkyl tail but the size of their polar head is larger than that of the alkyl groups. We have shown previously that such asymmetric surfactant molecules aggregate and adsorb in cylindrical and spherical morphologies on polar surfaces.[22] The basic principle behind our theoretical model is that, upon adsorption, the most energetically favorable morphology is attained, which depends on the relative strength of interactions between the polar head and the alkyl tail with the surface. If the alkyl tails have appreciable affinity for the surface, then the molecules adsorb by "lying down" on the surface. However, such a configuration occupies a larger surface area. A "standing-up" configuration with only the polar group in contact with the surface will allow more molecules to adsorb on the surface. Thus, by comparing the overall energetics associated with the two configurations that cover the entire adsorbing surface, one can predict the favorable adsorbed configuration in different cases.[21] In the case of asymmetric surfactant molecules, the standing-up configuration results in morphologies with signatures of full cylinders and the lying-down configuration shows signatures of partial spheres. In this paper, we first describe our theoretical model and then discuss results of the simulations performed to check the validity of the model.

2. THEORETICAL MODEL

Consider a surfactant molecule with a polar head of size σ_p and comprised of n alkyl groups in the tail, with each alkyl group of size σ. Let ε^S_{HS} and ε^S_{TS} denote the interaction strengths of the polar headgroup (H) and an alkyl tail group (T) with the surface respectively in the standing-up (S) configuration. ε^L_{HS} and ε^L_{TS} are analogously defined for the lying-down (L) configuration. Let l be the length of the alkyl tail. For a configuration of molecules standing up on the surface, the energy is given by

$$E^S = \varepsilon^S_{HS} P^S \frac{A}{A^S_m} \tag{1}$$

where P^S is the packing fraction of the molecules adsorbed on the surface, A is the total area of the surface, and A^S_m is the area occupied by a molecule in the standing-up configuration. P^S is given by

$$P^S = N^S \frac{A^S_m}{A} \tag{2}$$

where N^S is the number of molecules adsorbed in the standing-up configuration. The energy associated with the lying-down configuration is given by

$$E^L = (\varepsilon^L_{HS} + n\varepsilon^L_{TS}) P^L \frac{A}{A^L_m} \tag{3}$$

where P^L is the packing fraction of the adsorbed molecules and A^L_m is the area occupied by a molecule in the lying-down configuration. P^L is given by

$$P^L = \frac{N^L A^L_m}{A} \tag{4}$$

where N^L is the number of molecules in the lying-down configuration in the first adsorbed layer on the surface. The area occupied per molecule in the two configurations can be calculated from the geometry of the molecule

$$A^S_m = \pi\left(\frac{\sigma_p}{2}\right)^2 \tag{5}$$

$$A^L_m = l\sigma + \pi\left(\frac{\sigma_p}{2}\right)^2 \tag{6}$$

If the interactions of the polar head and the alkyl tail groups with the surface are independent of the adsorbed configuration, then the subscripts L and S can be dropped from the interaction energy terms. In that case, the ratio of energies in the two configurations is given by

$$\frac{E^L}{E^S} = \frac{(\varepsilon_{HS} + n\varepsilon_{TS}) P^L A^S_m}{\varepsilon_{HS} P^S A^L_m} \tag{7}$$

Thus, the equilibrium adsorbed configuration depends on the strength of interactions of the polar head and the alkyl tail with the surface, as well as the molecular geometry. The model predicts that, when $E^L > E^S$, the lying-down configuration is preferred over the standing-up configuration and vice versa. This theoretical model is valid under the conditions when the adsorption is strongly favored. Therefore, one would expect the surface to be maximally covered and $P^L \approx P^S$. With the assumption that $P^L \approx P^S$, eq 7 can be applied without determining the equilibrium number of adsorbed molecules per unit area, and thus precludes the need to fit any data to the model to make predictions. It should be noted that, since our theoretical model is only based on molecular geometry, it does not require quantities needed to describe geometrical shapes of the adsorbed morphologies, unlike in previous works.[15,16] Therefore, while our theoretical model does not attempt to predict the overall adsorbed morphologies directly, it explains the configurations that are attained by individual adsorbing molecules, which in turn manifest different adsorbed morphologies.

3. SIMULATION SYSTEM AND METHODS

To test the validity of the theoretical model, we have performed Langevin dynamics simulations of adsorption of asymmetric surfactant molecules on polar surfaces. Surfactant molecules are represented by a coarse-grained bead−spring model employed previously,[21,22] wherein the first bead represents the polar headgroup and the remaining beads represent the alkyl tail. The size of the polar head bead is taken as twice that of an alkyl bead, that is, $\sigma_p = 2\sigma$. The alkyl tail is represented by $n = 19$ alkyl beads connected to each other via harmonic bond and angle potentials with an equilibrium bond length of 0.3σ and an equilibrium angle of 180°. The polar head bead is connected to the alkyl tail with a harmonic bond potential of equilibrium length 1.5σ. The interactions between the surface and the beads are modeled via a 9-3 potential, which is essentially an integrated Lennard-Jones (LJ) potential

https://dx.doi.org/10.1021/acs.jpcb.0c02681
J. Phys. Chem. B XXXX, XXX, XXX−XXX

over a semi-infinite slab of LJ particles, which allows us to treat the surface as a smooth plane. The well-depths of the 9-3 potentials for the head bead and the alkyl tail beads are ε_{HS} and ε_{TS}, respectively. Simulations are performed for different values of ε_{HS} and ε_{TS} in order to obtain the equilibrium morphologies and compare them against the predictions of our theoretical model. Interactions between any two alkyl beads are modeled via a LJ potential with the potential well-depth of ε_{TT}. Interactions between a polar bead and an alkyl bead are modeled via a purely repulsive Week−Chandler−Andersen potential. Solvent is treated implicitly in the simulations. The effect of solvent is incorporated by performing Langevin dynamics simulations. All quantities are reported in reduced units. Thermal energy, k_BT, is taken as the unit of energy, σ is taken as the unit of length, and mass of an alkyl bead, m, is taken as the unit of mass. To test the theoretical prediction, ε_{HS} is varied from 3 to 5 k_BT. This range of values matches the typical binding energies that have been calculated for polar groups on metal surfaces.[23] ε_{TS} is varied from 0 to 0.65 k_BT. As in our previous work,[21] the potential well-depth of the interaction between two alkyl beads is set to ε_{TT} = 0.065 k_BT. For this value of ε_{TT}, the overall hydrophobic interaction between two alkyl tails is of the order of k_BT.[24] The time step and the damping parameter for the Langevin dynamics simulations are $0.001\ \sigma\left(\frac{m}{k_BT}\right)^{1/2}$ and $0.1\ \sigma\left(\frac{m}{k_BT}\right)^{1/2}$. The force constants associated with the bond and angle harmonic potentials are 100 k_BT/σ^2 and 50 k_BT/rad^2, respectively. The size of the simulation box is $26.93\sigma \times 26.94\sigma \times 40.0\sigma$. These dimensions are chosen to ensure that the volume density of the surfactants in our system is equal to that in our previous work on symmetrical, linear surfactant molecules.[21] The total number of molecules in the simulation box is 400.

To apply the theoretical model (eq 7), one needs to determine the values of P^L and P^S from the simulations, which depend on the values of N^L and N^S, respectively. The values of N^L and N^S are determined by counting the number of molecules in the first adsorbed layer of the two configurations when the surface is maximally covered by the molecules. In our simulations (discussed later), we find that $P^L \approx P^S$, and therefore, eq 7 does not require any fitting parameters to be calculated from the simulations. The condition of $P^L \approx P^S$ is not surprising because our theoretical model is valid under the assumption that the adsorption of molecules is strongly favored and as a result the surface is expected to be maximally covered.[21]

4. RESULTS AND DISCUSSION

4.1. Validating the Theoretical Model. In the first layer, the surfactant molecules may adsorb either in the lying-down or standing-up configuration depending on the strength of their interactions with the surface. Figure 1 shows results of the simulations performed by choosing different values of ε_{HS} and ε_{TS}. Every data point in the figure corresponds to the equilibrium adsorbed configuration of the surfactant molecules for a given (ε_{TS}, ε_{HS}). The figure also shows prediction of the theoretical model (eq 7) for which $E^L = E^S$, that is, when the energy associated with the lying-down and the standing-up configuration is equal. For a given value of ε_{TS}, if the ε_{HS} is above the theoretical line, then the standing-up configuration is expected to be preferred over the lying-down configuration. Figure 1 shows that this is indeed the result that is obtained in our simulations, implying that our theoretical model is quantitatively accurate in predicting the adsorbed configurations of asymmetrical surfactant molecules on polar surfaces. Interestingly, for some data points close to the theoretical line in Figure 1, the standing-up and lying-down configurations coexist. These data points are labeled as "Mixed" in Figure 1.

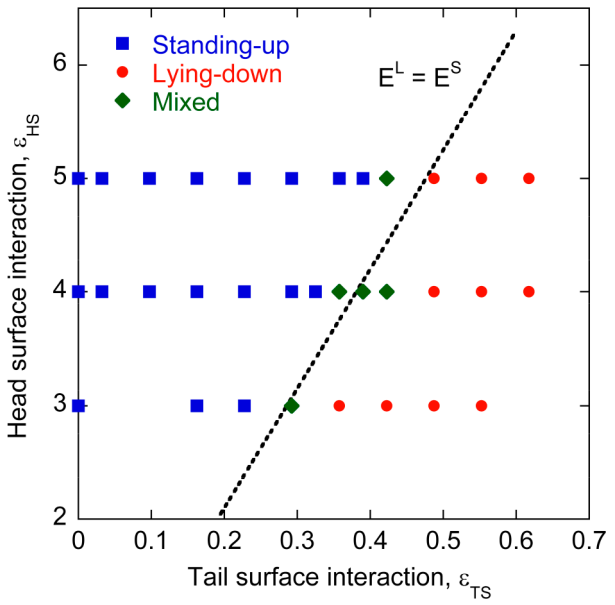

Figure 1. Results of equilibrium adsorbed configurations obtained in Langevin dynamics simulations performed for different values of (ε_{TS}, ε_{HS}). The theoretically predicted condition of $E^L = E^S$ is also shown. The results from the simulations are found to be in quantitative agreement with the theory.

The standing-up and lying-down configurations are identified from the significantly different orientational distributions of the adsorbed molecules. This is illustrated in Figure 2a, which shows the distribution of angles in these two configurations. The angle θ is defined as the angle that the vector joining the terminal alkyl bead to the polar head bead forms with the plane of the surface. The distribution of θ shown in Figure 2a has been normalized by cos θ. In the lying-down configuration, the distribution has a peak of $\theta \approx 7°$, which is as per our expectation because the surfactant molecule is 7.2σ long and the polar head is 1σ larger than the alkyl bead. On the other hand, in the standing-up configuration, the distribution is broad at ±90°. For the standing-up configuration, the distribution does not go to zero for any θ, implying that the adsorption morphology is like a (squished) cylinder/sphere. Figure 2b shows the distribution of the center-of-mass of the molecules in the two adsorbed configurations shown in Figure 2a. The two configurations have different center-of-mass distributions as expected. The lying-down configuration has a sharp peak at 1σ from the surface, whereas the standing-up configuration has a peak at 5.4σ from the surface. The θ- and center-of-mass distributions of different (ε_{TS}, ε_{HS}) close to the theoretical line are shown in Figures S1−S7 (Supporting Information). A snapshot of the adsorbed morphologies that result from the standing-up and lying-down configurations is shown in Figure 3.

To visualize the adsorption morphologies, we have generated "instantaneous interface" snapshots of the adsorbed molecules[25] (Figure 4). In instantaneous interfaces, a continuous mass-density field is generated by applying a

https://dx.doi.org/10.1021/acs.jpcb.0c02681
J. Phys. Chem. B XXXX, XXX, XXX−XXX

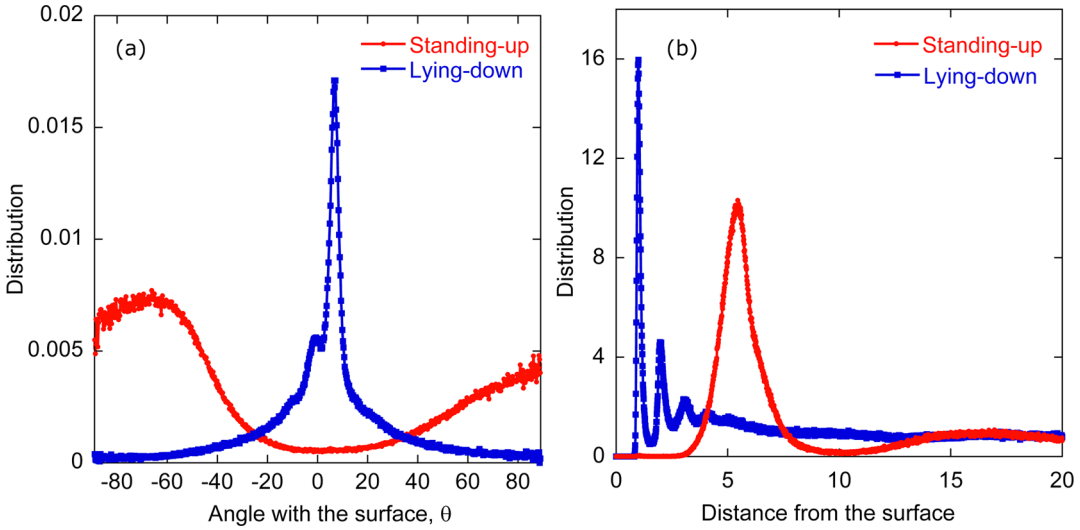

Figure 2. (a) Distribution of the angle that the adsorbed molecules make with the surface for (ε_{TS}, ε_{HS}) = (0.23, 5) (red color) and (ε_{TS}, ε_{HS}) = (0.55, 5) (blue color). For (ε_{TS}, ε_{HS}) = (0.23, 5), the molecules attain a standing-up configuration, whereas, for (ε_{TS}, ε_{HS}) = (0.55, 5), the molecules attain a lying-down configuration. (b) Distribution of the center-of-mass of the molecules from the surface for (ε_{TS}, ε_{HS}) = (0.23, 5) (red color) and (ε_{TS}, ε_{HS}) = (0.55, 5) (blue color). The lying-down configuration shows a sharp peak at 1σ, while the standing-up configuration shows a peak at 5.4σ.

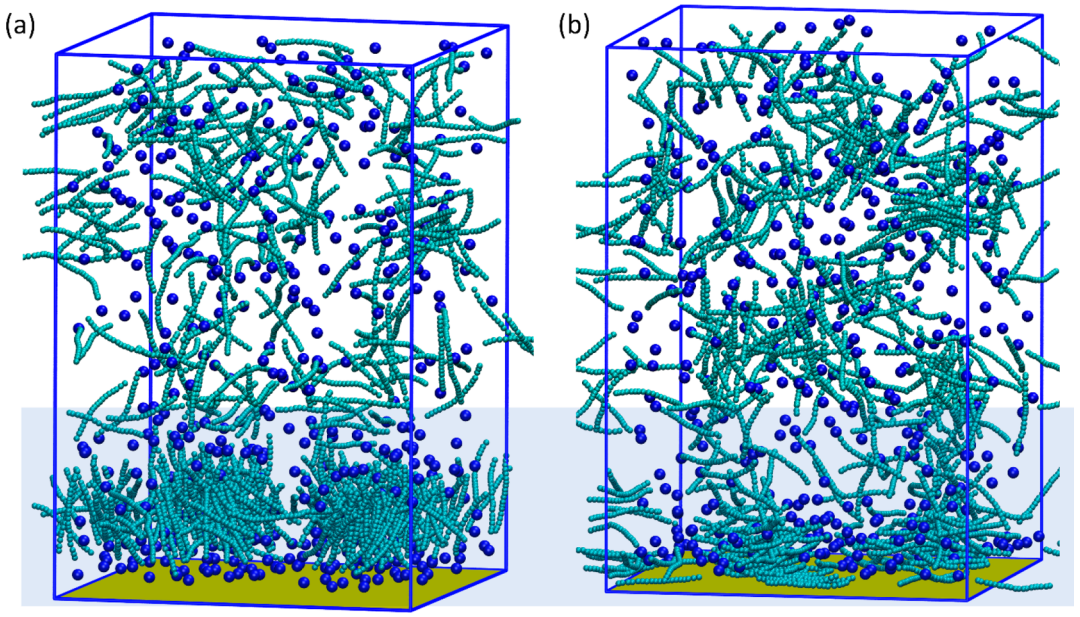

Figure 3. A snapshot of the equilibrated simulation system for (a) (ε_{TS}, ε_{HS}) = (0.23, 5) and (b) (ε_{TS}, ε_{HS}) = (0.55, 5) showing the standing-up and lying-down configurations, respectively. The region close to the surface has been shaded to highlight the adsorption region.

Gaussian distribution centered at the location of each particle in the system. At each point in space, contributions from these Gaussian distributions are added to determine the overall density field. Parts a and b of Figure 4 show top-view snapshots obtained from instantaneous interfaces for the standing-up [(ε_{TS}, ε_{HS}) = (0.23, 5)] and the lying-down configurations [(ε_{TS}, ε_{HS}) = (0.55, 5)], respectively. Details of the parameters employed for generating these interfaces are discussed in the figure caption. In the standing-up configuration, the instantaneous interfaces show the morphology to be close to cylindrical, whereas, in the lying-down configuration, the morphology more closely resembles spheres.

The kind of configuration that the surfactants attain upon adsorption affects the total number of adsorbed molecules, $\langle N \rangle$. Figure 5 shows the $\langle N \rangle$ for different values of ε_{HS} and ε_{TS}. In the standing-up configuration (shown by filled symbols), the number of molecules does not vary significantly with ε_{TS} for a given value of ε_{HS}. A sharp drop in $\langle N \rangle$ is observed as the configurations transition from the standing-up to the lying-down state (shown by open symbols). Mixed configurations (shown by the cross symbol), in which the lying-down and standing-up configurations coexist, have intermediate values of $\langle N \rangle$. $\langle N \rangle$ is smaller for the lying-down configurations, because the molecules occupy more surface area and so fewer molecules adsorb. It is an important result in the sense that, as the ε_{TS} increases for a given ε_{HS}, the total affinity of a surfactant molecule for the surface increases. However, our analysis shows that this increase in the affinity may result in a

https://dx.doi.org/10.1021/acs.jpcb.0c02681
J. Phys. Chem. B XXXX, XXX, XXX−XXX

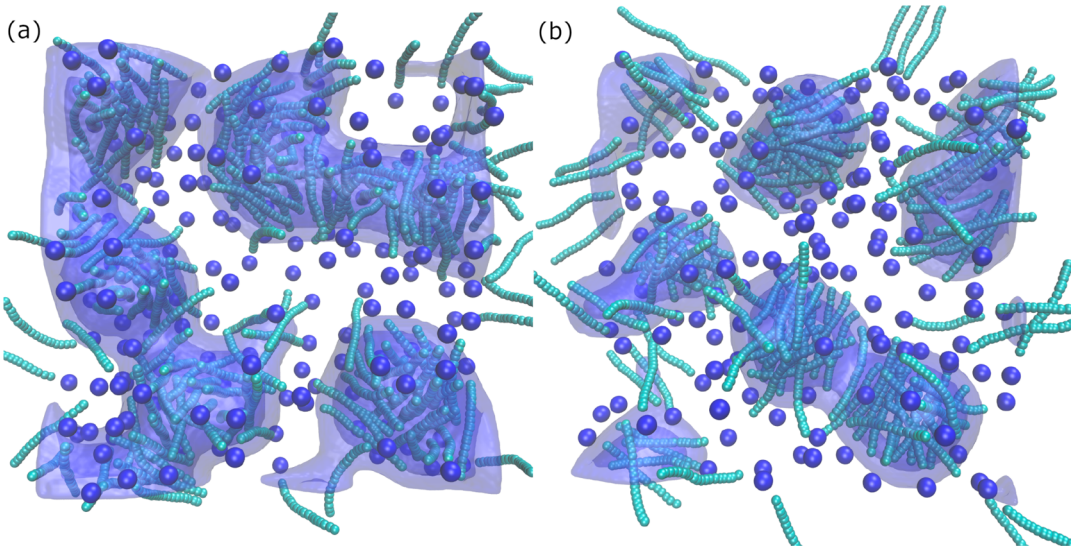

Figure 4. Top view of the adsorbing surface for (a) (ε_{TS}, ε_{HS}) = (0.23, 5) and (b) (ε_{TS}, ε_{HS}) = (0.55, 5). To visualize the morphology, instantaneous interfaces (blue surfaces) are generated by coarse-graining the density field by placing a normalized Gaussian function, $\phi(\mathbf{r}; \zeta) = (2\pi\zeta^2)^{-3/2}e^{-r^2/2\zeta^2}$, centered at the location $\mathbf{r}$ of each bead. The density field at any location is the summation of the contribution from the different Gaussian distributions. For our calculations, we choose $\zeta = 1.5\sigma$. The interface is formed by setting the lower and upper cutoff values of the density field as $0.5\sigma^{-3}$ and $0.7\sigma^{-3}$, respectively.

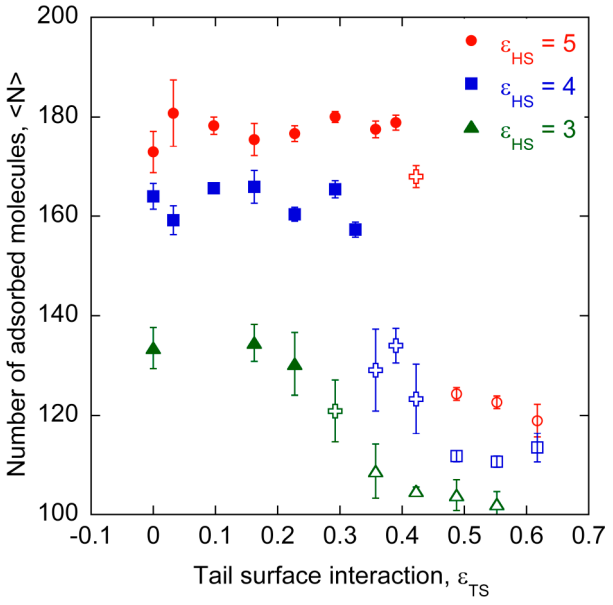

Figure 5. Equilibrium number of adsorbed molecules, $\langle N \rangle$, as a function of ε_{TS} for different values of ε_{HS}. The standing-up configurations are shown by filled symbols, and the lying-down configurations are shown by open symbols. The mixed configurations are shown by the cross symbol. Error bars are the standard deviation calculated from four different simulations.

decrease in $\langle N \rangle$ if the adsorbed configuration of the molecules changes.

4.2. Kinetic Pathways of the Formation of Adsorption Morphologies. Previous experiments have suggested that the organization of adsorbed surfactants in different morphologies may follow two different kinetic pathways. In the first pathway, the molecules initially adsorb by lying down on the surface, and then, as more adsorption occurs, they undergo an orientational transition to stand up on the surface. In the second pathway, the molecules adsorb in the standing-up configuration to form islands. These islands grow and eventually coalesce to form the adsorption layer. Both of these kinetic pathways are observed in our simulations, and the preferred pathway depends on the relative magnitudes of ε_{TS} and ε_{HS}. Figure 6a shows the distribution of the angle, θ, at different times during the adsorption process for the case when (ε_{TS}, ε_{HS}) = (0.39, 5). For this set of interactions, the molecules are expected to attain the standing-up configuration as per Figure 1. The first time period, t_1, shows the θ-distribution to be sharply peaked at 7°, which is a signature of the lying-down configuration. There is a fraction of the molecules that is standing up on the surface, as the distribution is nonzero at $\theta = \pm 80°$. Figure 6b shows the distribution of the center-of-mass of the molecules from the surface. For the time period t_1, the distribution in Figure 6b has peaks at 1σ and 5.4σ from the surface, indicating that some molecules are lying down while some are standing up on the surface. The time period t_1 is from time 0 to $8.5 \times 10^4\, \sigma\left(\frac{m}{k_B T}\right)^{1/2}$, wherein the number of adsorbed molecules, N, increases from 0 to 150. The surface coverage from adsorbed molecules is close to 90% by the end of t_1 (Figure S8, Supporting Information). In the second time period, t_2 (from 8.5 to $17 \times 10^4\, \sigma\left(\frac{m}{k_B T}\right)^{1/2}$), it is observed that the peaks corresponding to the lying-down configuration are reduced in Figure 6a and b, implying that more molecules now stand up on the surface. N increases from 150 to 170 in this period. The period t_3 is from 25.5 to $34 \times 10^4 \left(\frac{m}{k_B T}\right)^{1/2}$. It is observed that the signatures of the lying-down configuration are now absent, implying that all of the adsorbed molecules are standing up on the surface. Thus, for this value of (ε_{TS}, ε_{HS}), the kinetic pathway involves an initial adsorption of the surfactant molecules in the lying-down configuration, which is followed by a gradual orientational transition to the standing-up configuration. This kind of kinetic pathway is observed for the state points that are close to the

https://dx.doi.org/10.1021/acs.jpcb.0c02681
J. Phys. Chem. B XXXX, XXX, XXX−XXX

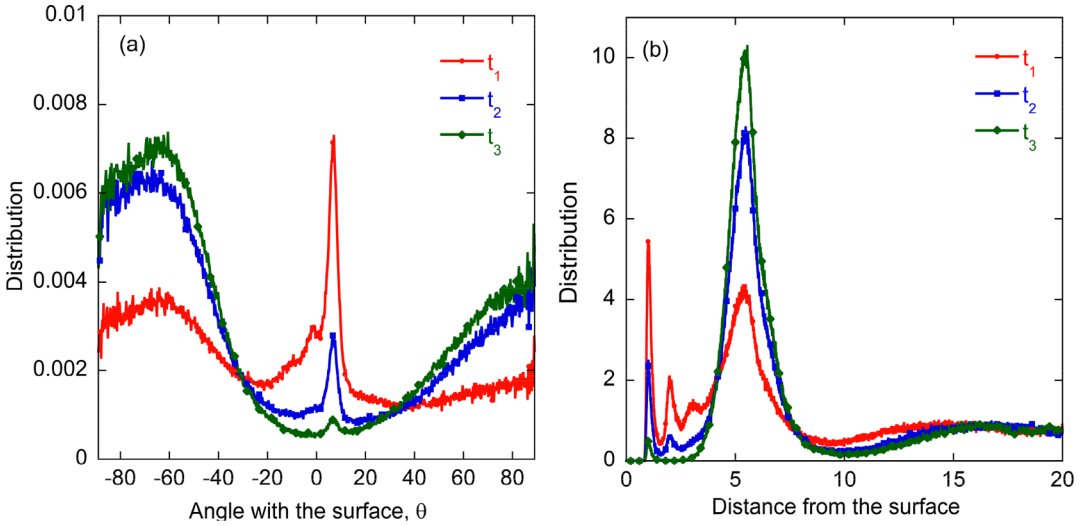

Figure 6. Kinetics of adsorption of the surfactants for (ε_{TS}, ε_{HS}) = (0.39, 5). (a) shows the distribution of the angle that the molecules form with the surface, θ at different time periods ($t_1 < t_2 < t_3$). (b) shows the distribution of the distance of the center-of-mass of the molecules from the surface for the same time periods. These graphs show that the kinetics of adsorption involve a standing-up to a lying-down orientational transition.

theoretical line of $E^L = E^S$. For such state points, the lying-down configuration is energetically comparable to the standing-up configuration.

To observe the second kind of kinetic pathway, one can analyze the adsorption kinetics of a data point for the standing-up configuration that is away from the theoretical line of $E^L = E^S$. Figure 7 shows the distribution of the angle θ at different

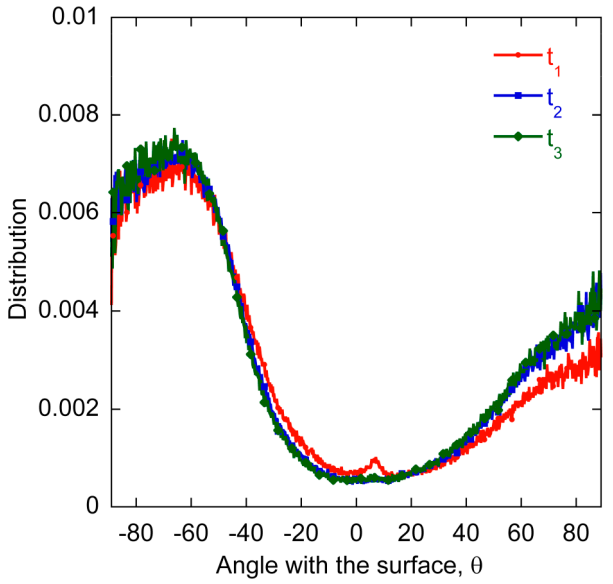

Figure 7. Kinetics of adsorption of the surfactants for (ε_{TS}, ε_{HS}) = (0.23, 5). The figure shows the distribution of the angle that that the molecules form with the surface, θ at different time periods ($t_1 < t_2 < t_3$). At all times, the distribution of the θ represents the standing-up configuration.

times during the adsorption process for the case when (ε_{TS}, ε_{HS}) = (0.23, 5). In this case, the θ-distribution at all time periods t_1, t_2, and t_3 matches with that of a standing-up configuration. Thus, in this case, the kinetic pathway involves the formation of islands of standing-up molecules. These islands grow and coalesce as the adsorption increases with time.

To identify the islands on the surface, the following procedure is employed: the surface is divided into cubes of side 0.2σ. All alkyl beads within 1.5σ and all polar beads within 3σ from the surface are projected onto the plane of the surface. The cubes that are within 0.8σ ($0.8\sigma_p$) from the alkyl (polar) beads are labeled as occupied. All the occupied cubes adjacent to each other are considered part of an island. Figure 8 illustrates the formation and growth of islands of adsorbed molecules for (ε_{TS}, ε_{HS}) = (0.23, 5). Figure 8a shows the number of islands as a function of N. A large number of islands form on the surface initially. As N increases, these islands grow and coalesce into one another. The large fluctuation in the number of islands for a given value of N indicates that many islands break and form during the course of adsorption. This is further evidenced in Figure S9 (Supporting Information), wherein the number of islands is plotted as a function of total surface coverage. It is observed that, for a given surface coverage, there is fluctuation in the number of islands. For the same trajectory as shown in Figure 8a, Figure 8b tracks the size of the largest island as a function of N. The size is shown in terms of the fraction of the total surface area covered by the largest island. It is observed that the largest island grows as N increases.

5. CONCLUSIONS

In this work, we have developed a theoretical model to predict adsorbed configurations of surfactant molecules on polar surfaces. We have focused on asymmetric surfactant molecules that have a linear alkyl tail and a large polar headgroup. The theoretical model is based on the principle that, if the interactions of the polar head with the surface are much stronger than those of the alkyl tail with the surface, then the molecules attain a configuration in which they adsorb by standing up on the surface. This configuration allows more molecules to adsorb in comparison to the lying-down configuration and thus lowers the overall energy of the system. On the other hand, if the interactions of the alkyl tail with the surface are strong, the molecules adsorb in the lying-down configuration. Due to the asymmetrical geometry of the surfactant molecules, the molecules attain a cylindrical

https://dx.doi.org/10.1021/acs.jpcb.0c02681
J. Phys. Chem. B XXXX, XXX, XXX−XXX

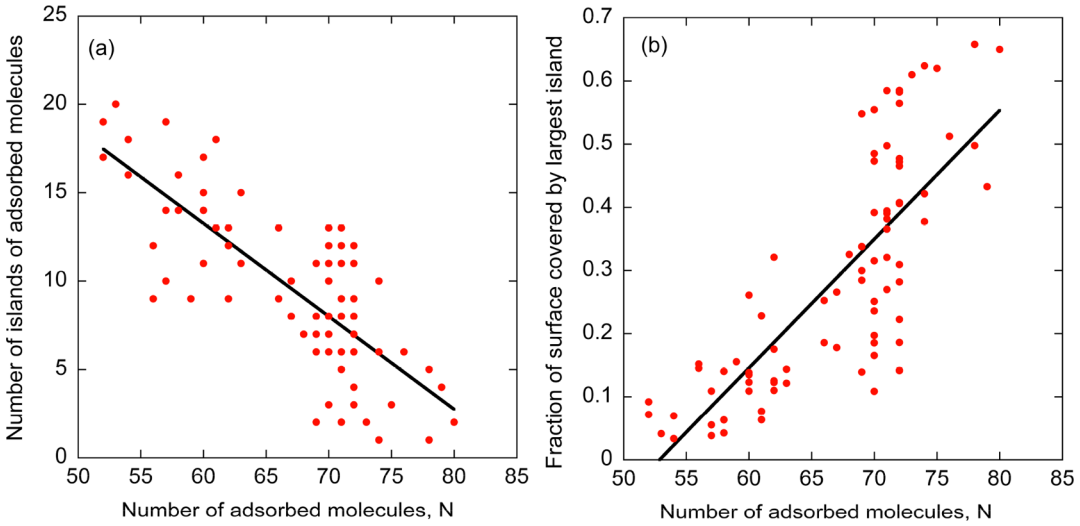

Figure 8. Formation of islands of adsorbed molecules during the adsorption process in the case of (ε_{TS}, ε_{HS}) = (0.23, 5). (a) Number of islands as a function of the number of adsorbed molecules, *N*, and (b) fraction of the surface area covered by the largest island as a function of *N*. Best fit lines are shown as a guide to the eye.

morphology in the standing-up configuration and a partially spherical morphology in the lying-down configuration. Our simulations show that the theoretical model is quantitatively accurate in predicting the adsorbed configurations of surfactant molecules.

■ ASSOCIATED CONTENT

Supporting Information

The Supporting Information is available free of charge at https://pubs.acs.org/doi/10.1021/acs.jpcb.0c02681.

Figures S1−S7 show (a) the θ-distribution and (b) center-of-mass distribution of surfactant molecules for the following values of (ε_{TS}, ε_{HS}): (0.42, 5) [mixed], (0.32, 4) [standing up], (0.36, 4) [mixed], (0.42, 4) [mixed], (0.23, 3) [standing up], (0.29, 3) [mixed], (0.36, 3) [lying down]; Figure S8 shows the fraction of the surface covered by surfactant molecules as a function of the number of adsorbed molecules for (ε_{TS}, ε_{HS}) = (0.23, 5); and Figure S9 shows the number of islands as a function of the fraction of the surface covered (PDF)

■ AUTHOR INFORMATION

Corresponding Author

Sumit Sharma − *Department of Chemical and Biomolecular Engineering, Ohio University, Athens, Ohio 45701, United States;* orcid.org/0000-0003-3138-5487; Phone: +1-740-593-1425; Email: sharmas@ohio.edu

Author

Xueying Ko − *Department of Chemical and Biomolecular Engineering, Ohio University, Athens, Ohio 45701, United States;* orcid.org/0000-0002-7744-7690

Complete contact information is available at: https://pubs.acs.org/10.1021/acs.jpcb.0c02681

Notes

The authors declare no competing financial interest.

■ ACKNOWLEDGMENTS

This work is supported by the National Science Foundation (NSF) CBET grant 1705817 and the NSF XSEDE grant DMR190005. The authors thank researchers at the Institute for Corrosion and Multiphase Technology (ICMT) for useful discussions. X.K. thanks the support of Ohio University Graduate College Fellowship for the year 2018−2019. S.S. thanks Ohio University for covering the computational costs for resources provided by the Ohio Supercomputer Center.

■ REFERENCES

(1) Popoola, L. T.; Grema, A. S.; Latinwo, G. K.; Gutti, B.; Balogun, A. S. Corrosion Problems During Oil and Gas Production and its Mitigation. *Int. J. Ind. Chem.* **2013**, *4*, 35.

(2) Li, J.; Kaifer, A. E. Surfactant Monolayers on Electrode Surfaces: Self-Assembly of a Viologen Derivative having a Cholesteryl Hydrophobic Residue. *Langmuir* **1993**, *9* (2), 591−596.

(3) Marshall, S. T.; O'Brien, M.; Oetter, B.; Corpuz, A.; Richards, R. M.; Schwartz, D. K.; Medlin, J. W. Controlled Selectivity for Palladium Catalysts using Self-Assembled Monolayers. *Nat. Mater.* **2010**, *9* (10), 853.

(4) Murphy, C. J.; Sau, T. K.; Gole, A. M.; Orendorff, C. J.; Gao, J.; Gou, L.; Hunyadi, S. E.; Li, T. Anisotropic Metal Nanoparticles: Synthesis, Assembly, and Optical Applications. *J. Phys. Chem. B* **2005**, *109*, 13857−13870.

(5) Knag, M.; Sjöblom, J.; Øye, G.; Gulbrandsen, E. A Quartz Crystal Microbalance Study of the Adsorption of Quaternary Ammonium Derivates on Iron and Cementite. *Colloids Surf., A* **2004**, *250* (1−3), 269−278.

(6) Singh, H.; Sharma, S. Disintegration of Surfactant Micelles at Metal-Water Interfaces Promotes their Strong Adsorption. *J. Phys. Chem. B* **2020**, *124* (11), 2262−2267.

(7) Kurapati, Y.; Sharma, S. Adsorption Free Energies of Imidazolinium-type Surfactants in Infinite Dilution and in Micellar State on Gold Surface. *J. Phys. Chem. B* **2018**, *122*, 5933−5939.

(8) Sharma, S.; Ko, X.; Kurapati, Y.; Singh, H.; Nešić, S. Adsorption Behavior of Organic Corrosion Inhibitors on Metal Surfaces—Some New Insights from Molecular Simulations. *Corrosion* **2019**, *75* (1), 90−105.

(9) Xiong, Y.; Brown, B.; Kinsella, B.; Nešic, S.; Pailleret, A. Atomic Force Microscopy Study of the Adsorption of Surfactant Corrosion Inhibitor Films. *Corrosion* **2014**, *70* (3), 247−260.

(10) Poirier, G. E.; Pylant, E. D. The Self-Assembly Mechanism of Alkanethiols on Au (111). *Science* **1996**, *272* (5265), 1145−1148.
(11) Jaschke, M.; Butt, H.-J.; Gaub, H. E.; Manne, S. Surfactant Aggregates at a Metal Surface. *Langmuir* **1997**, *13* (6), 1381−1384.
(12) Manne, S.; Cleveland, J. P.; Gaub, H. E.; Stucky, G. D.; Hansma, P. K. Direct Visualization of Surfactant Hemimicelles by Force Microscopy of the Electrical Double Layer. *Langmuir* **1994**, *10* (12), 4409−4413.
(13) Patrick, H. N.; Warr, G. G.; Manne, S.; Aksay, I. A. Surface Micellization Patterns of Quaternary Ammonium Surfactants on Mica. *Langmuir* **1999**, *15* (5), 1685−1692.
(14) Olivo, J. D.; Brown, B.; Young, D.; Nešić, S. Effect of Corrosion Inhibitor Alkyl Tail Length on the Electrochemical Process Governing CO2 Corrosion of Mild Steel. *Corrosion* **2019**, *75* (2), 137−139.
(15) Johnson, R. A.; Nagarajan, R. Modeling Self-Assembly of Surfactants at Solid/Liquid Interfaces. I. Hydrophobic Surfaces. *Colloids Surf., A* **2000**, *167* (1−2), 31−46.
(16) Johnson, R. A.; Nagarajan, R. Modeling Self-Assembly of Surfactants at Solid−Liquid Interfaces. II. Hydrophilic Surfaces. *Colloids Surf., A* **2000**, *167* (1−2), 21−30.
(17) Xu, S.; Cruchon-Dupeyrat, S. J. N.; Garno, J. C.; Liu, G.-Y.; Kane Jennings, G.; Yong, T.-H.; Laibinis, P. E. In Situ Studies of Thiol Self-Assembly on Gold from Solution using Atomic Force Microscopy. *J. Chem. Phys.* **1998**, *108* (12), 5002−5012.
(18) Woodward, J. T.; Doudevski, I.; Sikes, H. D.; Schwartz, D. K. Kinetics of Self-Assembled Monolayer Growth Explored via Submonolayer Coverage of Incomplete Films. *J. Phys. Chem. B* **1997**, *101* (38), 7535−7541.
(19) Doudevski, I.; Hayes, W. A.; Schwartz, D. K. Submonolayer Island Nucleation and Growth Kinetics during Self-Assembled Monolayer Formation. *Phys. Rev. Lett.* **1998**, *81* (22), 4927.
(20) Hayes, W. A.; Schwartz, D. K. Two-Stage Growth of Octadecyltrimethylammonium Bromide Monolayers at Mica from Aqueous Solution below the Krafft Point. *Langmuir* **1998**, *14* (20), 5913−5917.
(21) Sharma, S.; Singh, H.; Ko, X. A Quantitatively Accurate Theory to Predict Adsorbed Configurations of Linear Surfactants on Polar Surfaces. *J. Phys. Chem. B* **2019**, *123* (34), 7464−7470.
(22) Ko, X.; Sharma, S. Adsorption and Self-Assembly of Surfactants on Metal−Water Interfaces. *J. Phys. Chem. B* **2017**, *121* (45), 10364−10370.
(23) Kovačević, N.; Milošev, I.; Kokalj, A. How relevant is the adsorption bonding of imidazoles and triazoles for their corrosion inhibition of copper? *Corros. Sci.* **2017**, *124*, 25−34.
(24) Choudhury, N.; Pettitt, B. M. The Dewetting Transition and the Hydrophobic Effect. *J. Am. Chem. Soc.* **2007**, *129* (15), 4847−4852.
(25) Willard, A. P.; Chandler, D. Instantaneous Liquid Interfaces. *J. Phys. Chem. B* **2010**, *114* (5), 1954−1958.

https://dx.doi.org/10.1021/acs.jpcb.0c02681
J. Phys. Chem. B XXXX, XXX, XXX−XXX